NUCLEATE POOL BOILING INVESTIGATION ON A SILICON TEST SECTION WITH MICRO-FABRICATED CAVITIES

A. Sanna*, C. Hutter°, D.B.R. Kenning*, T.G. Karayiannis*, K. Sefiane°, R.A. Nelson[+]

*BRUNEL UNIVERSITY - West London, UB8 3PH, Uxbridge - UK
°UNIVERSITY of EDINBURGH, Edinburgh, EH9 3JL - UK
[+] LOS ALAMOS NATIONAL LABORATORY, Los Alamos, NM 87545 - USA

ABSTRACT

The basic mechanisms of nucleate boiling are still not completely understood, in spite of the many numerical and experimental studies dedicated to the topic. The use of a hybrid code allows reasonable computational times for simulations of a solid plate with a large population of artificial micro-cavities with fixed distribution. This paper analyses the guidelines for the design, through numerical simulations, of the location and sizes of micro-fabricated cavities on a new silicon test section immersed in FC-72 at the saturation temperature for different pressures with an imposed heat flux applied at the back of the plate. Particular focus is on variations of wall temperature around nucleation sites.

INTRODUCTION

Nucleate pool boiling has long been used as a very effective mechanism for heat removal. Several empirical and theoretical models have been proposed to predict wall superheat. Dhir [1] identified two different approaches for the past studies, based either on empirical or on mechanism-based correlations. An alternative approach based on creation of a mechanistic model for prediction of the nucleate boiling heat transfer, focusing mainly on bubble dynamics and related heat transfer mechanisms, was also described in this paper. In his model, assumption of a constant surface temperature led to a thermally decoupled plate. Stephan et al. [2, 3] proposed a model where heat and fluid flow are investigated considering transient temperature in the wall, but it was limited to the study of an isolated bubble. A numerical code based on a model similar to the one developed by Stephan is limited to cases of low heat fluxes or large spacing between sites so that they can be approximately considered thermally uncoupled.

A hybrid model can constitute an alternative approach: it combines the complete solution of the temperature field in the solid with simple physical models for heat removal, bubble growth and interactions between sites. A hybrid numerical code was first developed at Los Alamos National Laboratory (LANL) by Pasamehmetoglu and Nelson [4], and then modified at Ljubljana University [5]. An improved version of the code [6] is now used to investigate high heat flux pool boiling on a silicon plate in FC-72 with a large number of artificial cavities; experimental data (i.e. bubble growth time, bubble period, departure radius and wall superheat) for an isolated bubble are required as input data. Analysis of the results of simulations, and particularly variation in wall temperature and number of activation of the sites, will guide placement and choice of activation superheat of approximately 100 micro-fabricated cavities (or more) in a new test section (0.38 mm thick silicon, with variable input heat flux applied on the back surface, chip size 50 mm x 50 mm, heated area 37 mm x 40 mm, surface in contact with liquid 36 mm x 40 mm). Optical observation via high-speed camera will provide site activity and bubble departure radii. The test section will also contain 16 sensors (0.84 mm x 0.84 mm) located on the top surface and able to detect temperature variations with an error of ±0.5 K; they will provide support in measuring the activity of the sites when the visual observation is made difficult by the large number of bubbles. The design objective for this particular test section is to place the sites so that they interact thermally and cause local surface temperature variations that are detectable by the sensors. Data from the experiments will be used later for validation of the code.

The code, based on the FORTRAN language, solves the temperature three-dimensional space and time equation in a solid plate horizontally immersed in a liquid at saturation conditions, so that pool nucleate boiling may occur at fixed locations called nucleation sites that simulate artificial cavities on the top surface. The code combines the exact explicit solution of the temperature field in the solid plate with simplified models for heat removal from the top surface, for bubble growth mechanisms and for interactions between sites, including coalescence. Code flexibility includes the use of different plate materials and fluids (i.e. different heat transfer mechanisms) as well as variable potential activation site distributions on the upper surface with volumetric heat source or heat flux applied on the back of the plate [7].

Though the logic and syntax of the code have been recently rearranged by R.A. Nelson at LANL to increase the computational speed via parallelization, the maximum number of potential nucleation sites and plate dimensions are limited by computational power. Simulation of periods of 1 s, for a 36 mm x 24 mm x 0.38 mm silicon plate with approximately 100 nucleation sites (the size of the plate has been reduced in order to have faster simulations) on a dual processor (4 cores per processor) workstation takes of the order of 24 hours. The computational time strongly depends on the size and number of the cells and on the average number of sites active at the same time.

NUMERICAL MODEL

Input data

The code requires the definition of several input data. These values can be obtained either from experiments or from theoretical studies. In particular, the following data are required:

- Time scale and mesh management: simulated time, time step and mesh dimensions and characteristics.
- Characteristics of the plate: dimensions, conductivity, density, specific heat, initial temperature (T_{in}) and boundary conditions.
- Characteristics of the fluid: saturation temperature (T_{sat}), latent heat, density of vapour and liquid, specific heat, conductivity of the liquid.
- Heat transfer: imposed heat flux (q'') or volumetric heat source, heated area, heat transfer model and heat transfer coefficients (HTC) in the different areas, enhancing factors for heat transfer, as the general natural convection heat transfer enhancing factor (f_{enh}) and the local natural convection heat transfer enhancing factor ($f_{enh,loc}$).
- Bubble growth model: number and position of the potential activation sites (x_{NS}, y_{NS}), bubble departure radius (r_{bd}), activation temperature (T_{act}), possible uncertainty terms on the last two parameters, initial apparent contact angle (φ_0), angle decrease fraction (f_φ).

A more detailed description of some input data will be provided later in the paper.

Mesh management

At the beginning of the simulations, the plate is uniformly divided, horizontally into square cells (approximately 0.02 - 0.06 mm^2) arranged in a regular Cartesian grid, and vertically into layers with constant height (usually between 1 and 10 layers depending on the thickness of the plate). The distribution of cells is identically repeated for all the layers.

At each time step, the time-dependent three-dimensional temperature equation is solved consecutively for each cell starting from the bottom layer; an input heat source is applied, either as distributed volumetric heat generation or as a heat flux on the back of the whole plate or part of it. In this paper, only the constant heat flux condition has been applied.

Every time a site becomes active, i.e. when the temperature at fixed pre-determined locations on the top surface (activation sites, not necessarily located in correspondence with a square cell) exceeds an imposed value (activation temperature, T_{act}), a local mesh refinement process is applied identically to all the layers. The number of layers is not changed. The square cells around the activation site are replaced with finer ring-sector shaped cells (refined cells) arranged with circular symmetry in concentric rings over an area of radius r_m slightly bigger than the contact area radius r_c during the bubble growth. When the site deactivates, i.e. when the bubble radius reaches an imposed value (bubble departure radius, r_{bd}), an unrefinement process locally restores the original square cells. An example of mesh distribution for a case treated in the design section is shown in Fig.1. The 20 black dots correspond to potential (refined) nucleation sites, the 23 blue triangles to potential (unrefined) nucleation sites (only 23 of the 90 unrefined sites are shown here). Each violet dot corresponds to a centre of a cell (either square or ring-sector shaped), and each line to the connections between the

cells (used to calculate the cell area). It is clear that only 4 refined sites are active at the time considered (sites 4, 7, 10, 13); moreover, while site 10 has only four rings of refined cells, all the other sites have six. Distinction of refined and unrefined sites is explained in the next section.

In the original version of the code, r_m was fixed for each bubble growth according to the maximum contact area that occurred at the departure of the bubble, since the contact area was constantly increasing with time. Since mesh refinement is inhibited by the presence of already refined cells in the area that the new cells would occupy, the code was then reproducing unrealistic phenomena of alternating bubble growth at close-spaced nucleation sites. Additional simulations showed that this effect becomes more evident for larger square (w_{xy}) and refined cells sizes, since the not-overlapping rule assumes that activation or variation of the mesh radius for a site j may occur only if the distance d between j and each of the other sites (i) satisfies Eq.(1):

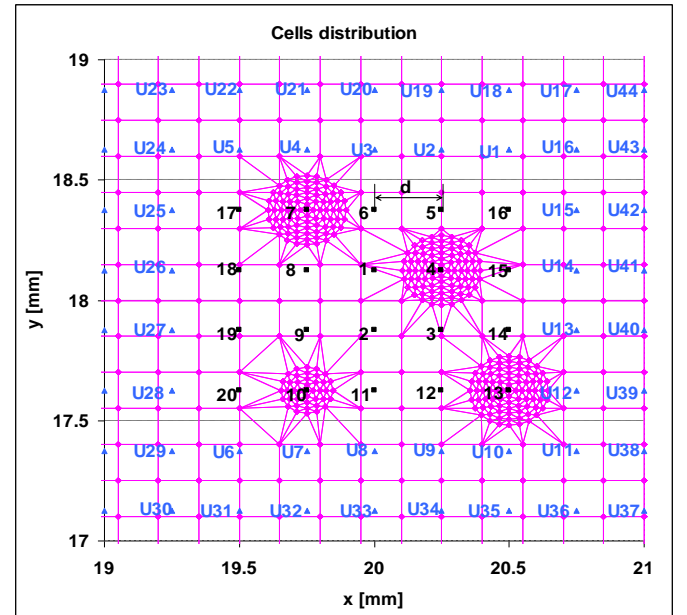$$d > 1.2\left(r_{mi} + r_{mj}\right) + 1.0w_{xy} \qquad (1)$$

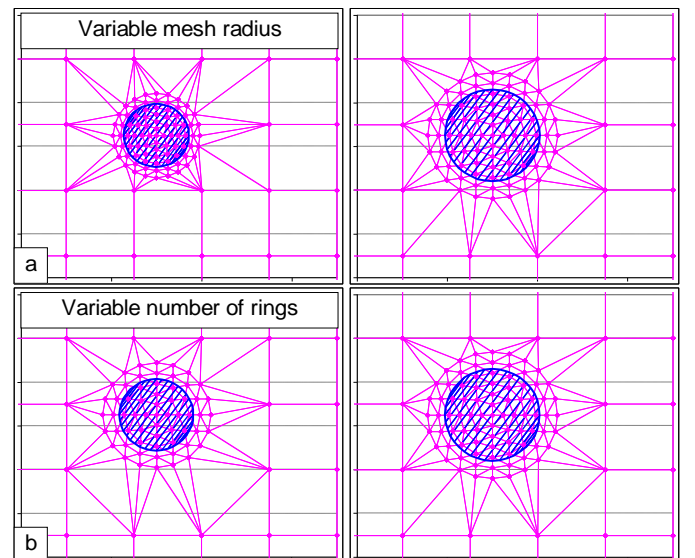**Figure 1: Mesh and nucleation sites distribution**

Figure 2: a) Variable mesh radius; b) Variable number of rings

However, increase in precision introduced a strong increase in computational time. The choice of a more representative physical model is then limited by computational constraints.

Two models (a) and (b), both using intermediate mesh refinement with variable mesh radius that can increase and decrease stepwise according to the contact area radius, have been implemented to reduce this problem to a smaller number of cases. The differences are:

a) Fixed number of refined cells per site, with consequent stepwise variable size for refined cells.

b) Fixed size of refined cells per site, with variable number of circular rings and then number of refined cells per site. This solution can be interpreted as the addition or removal of the external ring of refined cells when required, with no variation of position of inner refined cells during the whole bubble growth.

Fig.2a,b shows a comparison of the two models. The horizontal distribution of cells shown in the previous figure is compared to the contact area (in blue). Each violet dot corresponds to the centre of a cell. The mesh refinement process between different mesh radii requires for both solutions to temporarily restore the local distribution of square cells, with a partial loss of precision in calculation of temperature. Solution b), used for the simulations in this paper, allows the complete recovery of temperature between two intermediate mesh refinement processes since the position of the inner cells is not modified and the temperature values before refinement can be restored.

The use in case a) of a denser cell distribution when the contact area radius is small, with consequent much smaller cells size, reduces the maximum time step allowed; the size of the square cells must be chosen accordingly, in order to guarantee numerical stability of the code. Both processes cause significant delays in calculations. A large difference in size between square and refined cells also makes the refinement process more complex and consequently more time consuming.

For this reason, alternative approaches have been evaluated to speed up simulations, such as the use of a fixed fine distribution of square cells, or refined cells distributions fixed during the whole simulation. The first approach is not recommended since it does not allow a high definition in the contact area and it does not allow having the nucleation sites in any position. The second does not allow bubbles to grow at very close nucleation sites, limiting the choice of the location of the sites. A third compromise solution, currently under evaluation and applied in this paper, is described later.

Physical model

A fixed temperature distribution is initially applied to the plate (T_{in}). The lateral external surface of the cells at the edge of the plate is either adiabatic or at constant specified temperature. Adiabatic conditions are imposed on the bottom surface, while a heat transfer coefficient (HTC) varying at each time step and for each cell is imposed on the top surface.

Two different models are implemented at the moment for heat transfer at the top surface, as shown in Fig.3:

- contact line (CL) evaporation model as hypothesised by [2];
- micro-layer (ML) model as suggested by [8, 9].

The contact line evaporation model used in the code distinguishes four areas:

a) $HTC = 0$, for the inner contact area cells;

b) $HTC = HTC_{CL}$, for cells crossed by the triple contact line at each time step; this value is much higher than in the other areas, but much smaller than the theoretical value to be used if applied to a contact line area of theoretical dimensions; moreover, the value varies with the size of refined cells;

c) $HTC = f_{enh,loc} \cdot HTC_{NC}$: an enhanced natural heat transfer coefficient (usually with a local natural convection heat transfer enhancing factor $f_{enh,loc}$ equal to 2) for the cells immediately outside the contact area;

d) $HTC_{NC} = f_{enh} \cdot HTC_{NC,theor}$: a natural heat transfer coefficient, HTC_{NC}, is used for all the cells far from the contact area, according to Eq.(2) [10]. The general natural convection heat transfer enhancing factor (f_{enh}) (which may be <1) is calculated in order to match the time-averaged wall superheat as experimentally measured by a sensor. In the following examples, this value refers to the area around an active cavity (since the sensor area is generally bigger than the contact area) that can be considered an independent nucleation site [12]. In the future, measurements will refer to an area of the plate where boiling does not occur;
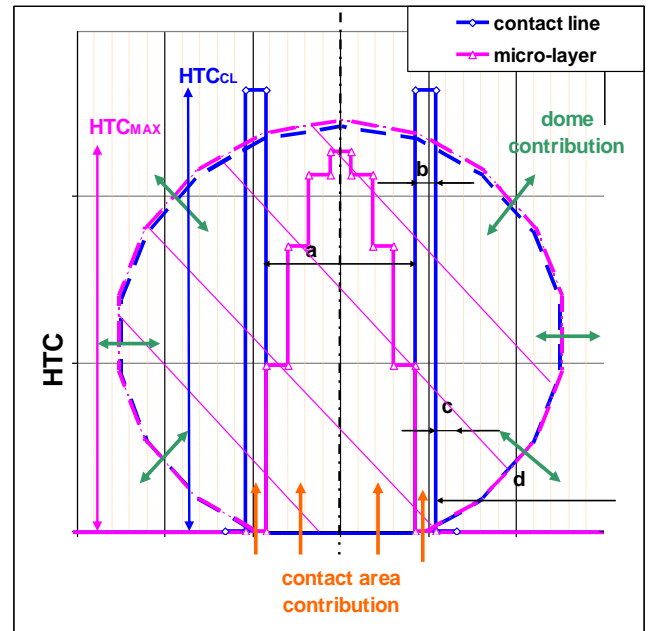

Figure 3: Heat transfer models and contributions
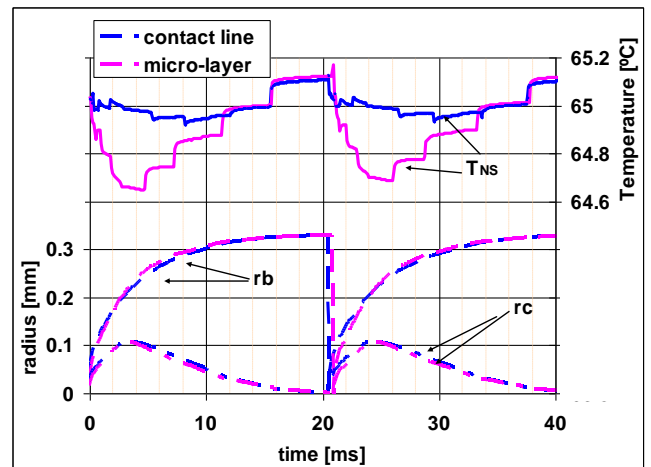

Figure 4: Comparison of temperature, bubble and contact radii histories for micro-layer and contact line models

$$HTC_{NC,theor} = 0.314(T_w - T_{sat})^{0.2} \quad [kW/m^2]. \quad (2)$$

The micro-layer model imposes:
a) a parabolic distribution with central peak (HTC_{MAX});
b) as for a);
c) $HTC = f_{enh,loc} \cdot HTC_{NC}$: as for the contact line model;
d) $HTC_{NC} = f_{enh} \cdot HTC_{NC,theor}$.

An illustrative comparison of the heat transfer coefficient profiles for a simulated 0.38 mm thick silicon plate in FC-72 along a diameter of the contact area for the two models is also shown in Fig.3; they refer to cases 1A and 1E described in the following section. The choice of the most appropriate model and related *HTC* values should be made on the basis of the characteristics of the plate and of the fluid and analysis of experimental data for single bubble growth and temperature profiles around the nucleation sites where available.

Heat removed from the contact area (a+b) is accounted as evaporation heat that contributes to the bubble growth, together with the heat exchanged at the dome of the bubble between the liquid and the vapour [7]. The bubble is supposed to grow as a truncated sphere of radius r_b, contact area radius r_c and variable apparent contact angle $\varphi(t)$, constant (φ_0) during the initial stage of bubble growth (i.e. until the bubble radius reaches a fixed angle decrease fraction, $f_\varphi = 0.6$ in this case, of the bubble departure radius) and linearly decreasing to zero by the ratio of bubble volume and maximum bubble volume afterward.

Illustrative temperatures at the nucleation site (T_{NS}) and bubble radii histories for an isolated nucleation site for the previous comparison are shown in Fig.4. Temperature variations at the centre of the contact area during bubble growth are much higher for the micro-layer model, due to the constant high heat transfer coefficient peak, than for the contact-line model, where there is a partial temperature recovery at the centre because of the zero heat transfer coefficient. HTC_{CL} and HTC_{MAX} have been tuned to match the experimentally measured growth time. Fig.4 also shows the comparison of contact area radii histories: the decrease after the first stage of the bubble growth is due to the reduction of the apparent contact angle.

A simple model for horizontal coalescence has also been implemented. Considering two adjacent sites (1 and 2) located at distance d and with bubble radii r_{b1} and r_{b2}, if contact between the projections of the domes of the bubbles on the horizontal plane occurs (i.e. $d < r_{b1} + r_{b2}$), and the radius of the bigger bubble (i.e. r_{b1}) is larger than twice the other one ($r_{b1} > 2r_{b2}$), bubble at site 2 coalesces (instantaneously disappearing) into bubble at site 1, which undergoes a sudden increase in volume now equal to the sum of the volumes of both the bubbles at the previous time step. If the bubble sizes are similar, bubbles are assumed to continue growing independently [6].

TEST SECTION DESIGN

The application of the code as a design tool requires the code to be run on high-speed commercial workstations (dual processor, 4 cores per processors) for approximately less than 24 hours, in the case of 100 sites and simulated time equal to 1s, allowing 30-40 activations per site at the most active sites.

The code requires the definition of the positions of potential activation sites (x_{NS}, y_{NS}), the activation temperature and then the activation wall superheat (ΔT_{act}) and the bubble departure radius (r_{bd}). To account the possible fluctuations related to the latter two inputs, uncertainty terms can be randomly introduced at each bubble growth for each of them. If not specified, this value is set to zero in the following simulations. ΔT_{act} is derived for each cavity by solution of Eq.(3) using data in Table 1.

$$\begin{cases} \log_{10} p\,(Pa) = 9.729 - \dfrac{1562}{T\,(K)} \\ \Delta p = \dfrac{2\sigma}{r_{cav}} \end{cases} \quad (3)$$

The original version of the code used a mesh refinement process for each site, strongly increasing the computational time and making the code unsuitable to simulate 100 potential nucleation sites, particularly if the mesh radius is larger than the average distance between sites, so that mesh refinement during the bubble growth becomes necessary. A simplified solution has been studied: the whole population of sites is divided in two groups, refined and unrefined. The refined ones are dealt as described before, and limited in number to a maximum of 20. The unrefined sites are dealt with a new procedure created to modify the heat transfer coefficients around an unrefined site in a pseudo circular distribution, in order to simulate a coarse contact area, without mesh refinement. The use of unrefined sites strongly reduces the computational time. Fig.5 shows a schematic comparison between the mesh defining the triple contact line area in the two cases. The coalescence model is not applied at present to unrefined sites.

For the unrefined cells, the heat transfer coefficient is automatically scaled; if the growth time is known from experiments, the *HTC* is scaled to match this input datum; otherwise, the code adjusts the *HTC* according to the refined to square cells size ratio. Nevertheless, the different cell size and distribution around refined and unrefined nucleation sites caused a sensible discrepancy between temperature profiles and bubble growth times between the two.

The design process can be divided in three parts:
1. Tuning of the model on the base of experimental results for an isolated bubble growth;
2. analysis of temperature variations and site activities after modification of the arrangement and characteristics of the sites applying the *HTC* as from previous tuning;

Table 1: Fluid data

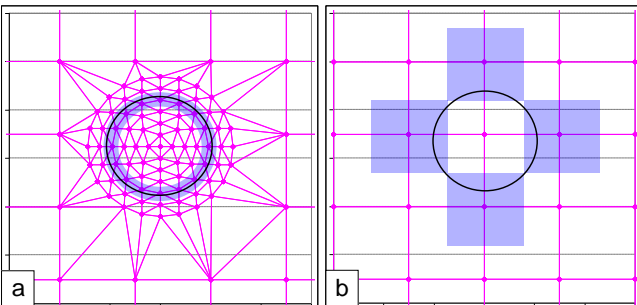| Material	T_{sat} [°C]	p [MPa]	σ [N/m]	r_{cav} [μm]	ΔT_{ACT} [K]
FC-72	57.15	0.100	~7.9·10⁻³	5	~0.94
				1	~4.49

Figure 5: Simulated triple contact line area for a
a) refined site;   b) unrefined site

3. conclusion and definition of the most appropriate disposition of sites in order to have the highest temperature variation during one bubble growth, so that site activity can be easily distinguished by the sensors.

Isolated bubble growth model

Two different 0.38 mm thick silicon test sections were available for experiments with FC-72 at atmospheric pressure:

- Test section #1: heated area 40 mm x 36 mm, with 16 micro-fabricated cavities (all of them 80 μm deep; 8 cavities with r_{cav} = 5 μm and 8 cavities with r_{cav} = 1.55 μm) with 16 temperature sensors (0.84 mm x 0.84 mm) located around the cavity on the top surface. The sites are arranged in two lines (each line with the same cavity depth) in pairs with variable inter-distance.
- Test section #2: heated area 10 mm x 15 mm, with 5 micro-fabricated cavities (r_{cav} = 5 μm and 40, 80 or 100 μm depth) located in the heated area of the top surface and 5 temperature sensors located on the back of the plate, as described in Hutter et al. [11].

Both the test sections have been simulated as a silicon plate (reduced to 16 mm x 11 mm x 0.38 mm to save computational time) with a slightly smaller central area (15 mm x 10 mm) heated on the back and with adiabatic conditions at the back and edges of the plate.

Two symmetrical cavities located in the middle of the plate at a distance of 3 mm have been simulated for test section #1 and one isolated cavity in the middle of the plate has been simulated for test section #2, reproducing respectively a pair of cavities 80 μm deep (r_{cav} = 5 μm) at the same simulated distance for test section #1 and cavity 3 (100 μm deep) for test section #2. Note that the code takes into account the different depth only by using the different experimental bubble growth times. The hypothesis of independent nucleation sites is in agreement with Zhang and Shoji [12].

A brief summary of results from 5 experimental cases at variable heat fluxes and superheats is shown in Table 2.

Four different simulations (A, B, C, D) have been run for each case, using the contact-line model and with variable initial contact angle φ_0 and angle decrease fraction f_φ. Fig.6 shows HTC_{CL} values (automatically adjusted by the code during simulations to match the experimental bubble growth times); their values are only illustrative, since they strongly depend on the refined cells sizes (and then indirectly on the bubble radius, initial contact angle and angle decrease factor) but they show a decrease with increasing φ_0 and f_φ.

Fig.7 shows the comparison between the different numerical and experimental results for case 1. The bubble radius history shows that the different apparent contact angle does not sensibly affect the bubble growth in simulations, while the final stage of bubble growth rate is severely flattened by increasing f_φ. The best matching simulations for case 1 are C for the initial stage of bubble growth and D

during the second stage, i.e. for φ_0 = 64° and f_φ between 0.9 and 0.97. The temperature T_{SEN}, averaged over an area on the top surface equal to the size of the sensor, shows good agreement with experimental data when the experimental data
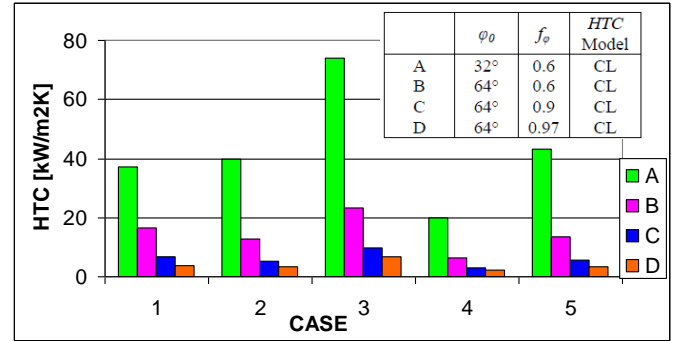

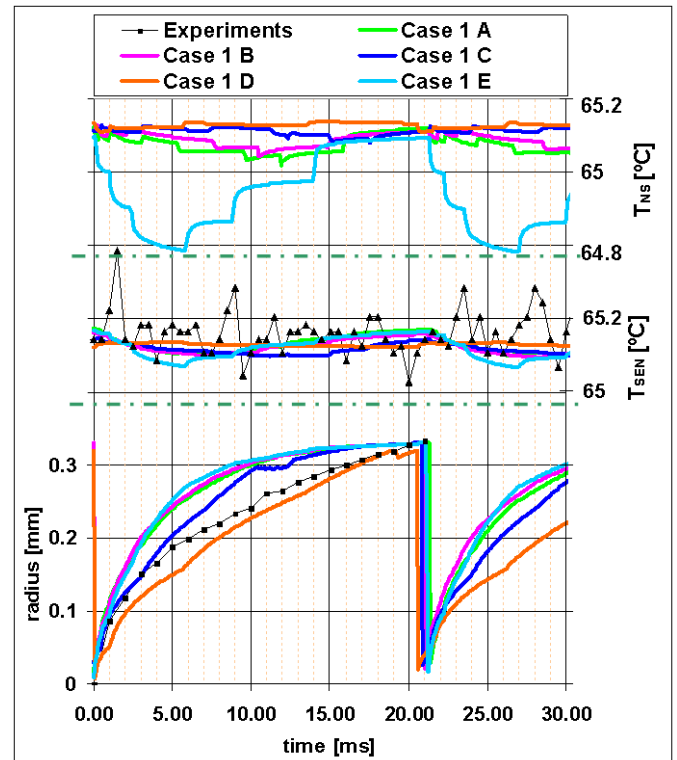**Figure 6: Heat transfer coefficients comparison**

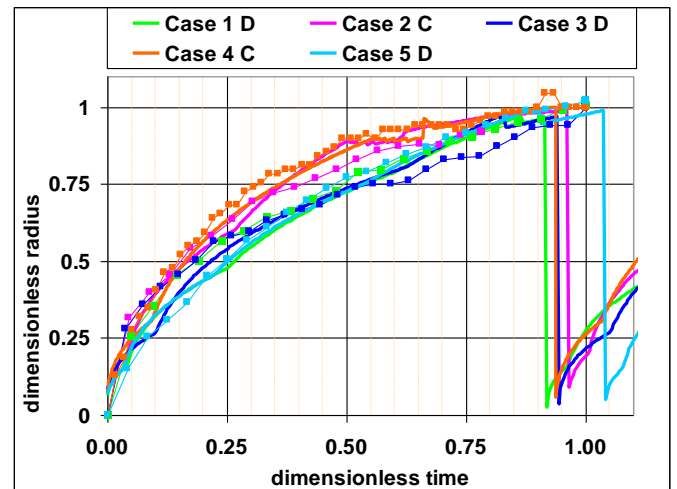**Figure 7: Radii and temperatures comparison between numerical and experimental results**

Figure 8: Dimensionless radii comparison between numerical and experimental results

Table 2: Summary of simulated cases

Case	r_{bd} mm	τ_g ms	ΔT_W K	f_{enh}	q'' kW/m²	Test section
1	0.33	21.0	8.1	1.16	4.48	1
2	0.24	23.0	4.8	1.14	2.36	1
3	0.19	27.0	1.4	0.98	0.46	1
4	0.16	59.0	1.3	1.97	0.85	2
5	0.35	24.0	10.1	2.66	13.4	2

are lowered by 0.42 K in the graph, an adjustment that is lower than the measurable error. No sensible variations in temperatures between the different simulations are evident, due to the large measuring area, at least twice the size of the maximum contact area. An additional simulation with φ_0 = 32° and f_φ = 0.6 but applying the ML model is also shown in Fig.7 (case 1E). This case shows much larger temperature variation at the nucleation site but similar trend for T_{SEN}. The simulations suggest that it will not be possible to define the most appropriate HTC model from measurement with the present size of sensors.

Fig.8 shows a very good agreement between numerical and experimental results for the dimensionless bubble radius (r_b/r_{bd}) versus dimensionless time (t/τ_g). The case shown for each simulation represents the best matching simulation, i.e. C for cases 2 and 4, and D for cases 1, 3 and 5. No waiting time or horizontal coalescence have been predicted in any of the simulated cases, contrary to experimental observations of significant waiting time for low heat fluxes (cases 3 and 4). Vertical bubble coalescence has not been simulated, since it did not occur during the considered experiments. The effect of this phenomenon on heat transfer must be experimentally verified and implemented in the future if necessary. Recent studies from Hutter et al. [13] showed that this phenomenon may affect the bubble volume at bubble departure, which would imply a variation in the evaporation heat in the code.

Experiments at sub-atmospheric pressure have been run for test section #1 to obtain larger bubble departure radii and consequent larger contact areas with possible larger variations in the measured temperature. Analysis of the temperature response of the sensor located at the same cavity over a long period, approximately 4 s (with applied heat flux of 8.6 kW/m^2), is shown in Fig.9. The pressure was reduced to 0.0463 MPa, leading to r_{bd} ~ 0.45 mm and τ_g ~ 10 ms. The uncertainty terms for bubble departure radius and superheat have been set equal to ±10%. The cavity experimentally showed large-period intermittent irregularities in activity, which could be reproduced artificially in the simulations by manually changing the activation temperature. Comparison with numerical results shows a good agreement, although variations in the simulations are faster and larger than in experiments, possibly due to hydro-dynamic effects in the liquid that are not modelled (but this does not explain either why the site becomes active or slower recovery when inactive).

Analysis of simulations

The number of activations and maximum variation in wall superheat at the nucleation site during the last simulated bubble growth (not necessarily occurring at the same time) for different spacing d between the potential nucleation sites is discussed here. The maximum variation in wall superheat is calculated for each nucleation site as the difference between the maximum and minimum temperatures reached during the last bubble growth for the considered site. This definition implies that the time when this parameter is evaluated can be strongly different for sites with low activity from sites with high activity, due for example to transient temperature effects. A higher maximum variation in temperature wall superheat implies a clearer identification of the activation of a nucleation site, constituting a leading parameter in the design process. The simulated time is 1.0 s. Case 1A has been used as the leading case, since case 1D would imply a larger

contact area radius to bubble radius ratio, which may emphasise a numerical influence on alternating bubble growth. Four simulations were run, using different spacing (d = 0.25, 0.5, 0.75 and 1.0 mm). HTC_{CL} values were recalculated in order to match the bubble growth time for an isolated bubble, according to the new size of the cells.

The distribution and numbering of the sites are the same as in Fig.1. Fig.10 shows the bubble radii for refined (violet) and unrefined (blue) sites at t ~ 230 ms: only ten refined sites become active at the same time, and they all grow in phase, apart from one (indicated by an arrow). The alternating behaviour, probably due to the numerical limitation (Eq.(1)), might also be caused by the inhibitory effects as reviewed by Kenning et al. [14]. By contrast, all the unrefined sites may be active at the same time, but they present more irregular behaviour. Analysis at different time steps shows that unrefined sites do not conserve symmetry, as refined sites do, and may be grow in clusters. A longer simulation period is required to analyse whether chaotic phenomena may occur.

Fig.11 shows the number of activations in 1.0 ms and the variation in superheat for each nucleation refined site. For d = 0.25 mm four refined sites (# 5, 10, 13, 17) activate ~30 times, while the others activate only once or twice (mainly at the beginning of the simulation). Similar behaviour is shown
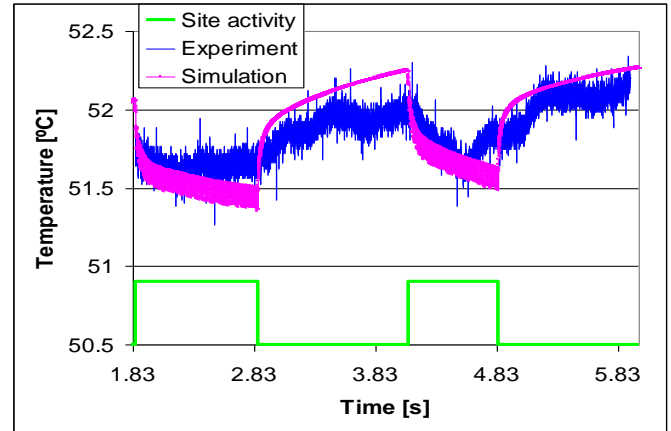
Figure 9: Comparison of the temperature response between experiment and simulation over a long period at sub-atmospheric pressure.
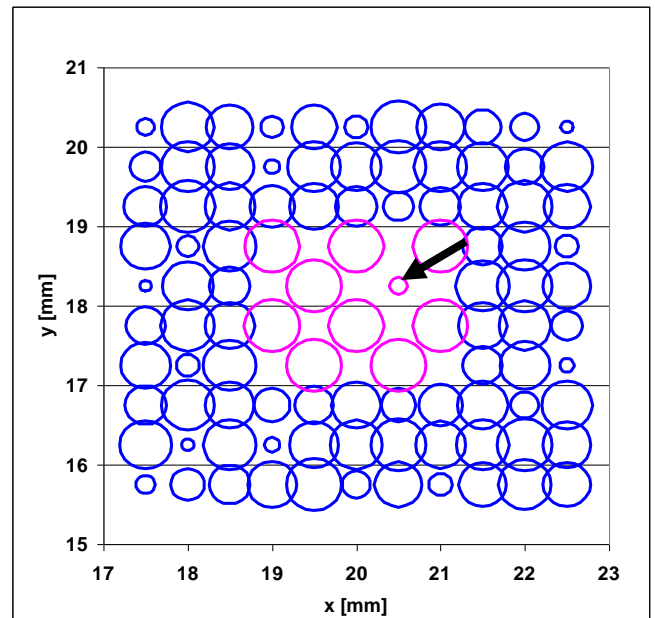
Figure 10: Bubble radii distribution (d = 0.5 mm)

for *d* = 0.5 mm, for which only half the sites regularly activate, while the others are constantly inhibited. The high variation in superheat for sites with low number of activations is probably due to the time when the site becomes active: in fact, superheat variation is larger if activation occurs at the beginning of the simulations, because of the initial temperature transient.

Comparison of the temperature histories at the same time for two adjacent refined sites (i.e. #5 and #6) shown in Fig.12 (*d* = 0.25 mm) and Fig.13 (*d* = 0.5 mm) highlights that there is almost no difference between the temperatures at adjacent nucleation sites even if one of the two is not active (if a site is not active the temperature is evaluated in the closest square cell) for both spacings. This indicates that the sites are strongly thermally interacting. Nevertheless, the increase of the spacing between nucleation sites implies a reduction of the average wall temperature and increase of the growth time relative to the experimental value for an isolated bubble. The temperature reduction is caused by an increased heat removal for *d* = 0.5 mm, due to the larger number of sites active at the same time relative to the case *d* = 0.25 mm.

Increase of the spacing (*d* = 0.75 and 1.0 mm) eliminates the alternating bubble growth effect: all the sites then have similar activity and superheat variation.

Fig.14 shows the number of activations and superheat variation for unrefined sites. The closer the site to the centre of the plate (i.e. the smaller the nucleation site #), the lower the number of activations and the higher the superheat variation during one bubble growth are. This effect, particularly evident for *d* = 0.25 mm, is probably due to the lateral conduction in the plate towards the edges, so that the central area has a lower wall superheat.

CONCLUSIONS

This paper aims to show the different capabilities of a hybrid numerical code that combines the complete three-dimensional space and time solution of the temperature field in a solid plate with simplified models and correlations to simulate the heat removal from the top surface and bubble growth during pool nucleate boiling. The code, first developed at Los Alamos National Laboratory and then modified at Ljubljana University, has been further improved, both from the numerical (it has been parallelised to speed up simulations) and physical (introduction of models for bubble growth, different heat transfer and horizontal coalescence) points of view. The code is now suitable to simulate interactions between a large number of nucleation sites, for different materials and fluids, and can be used as a design tool in studying the best distribution of micro-cavities to limit the maximum temperature variation when high heat fluxes are applied.

The code is tuned to correctly reproduce the bubble growth of an isolated bubble, on the base of experimental data used as input values, and it is able to simulate temperature variations over long periods of time, even if it is not able to reproduce irregularities in nucleation. The same conditions used for an isolated bubble are then applied to larger distributions of nucleation sites. A first investigation shows that at the moment the code may not be able to correctly simulate closely spaced nucleation sites due to numerical limitations on the mesh refinement process; a solution to remove or at least limit this effect is under study. Despite these limitations, temperature variations and activations of the sites have been
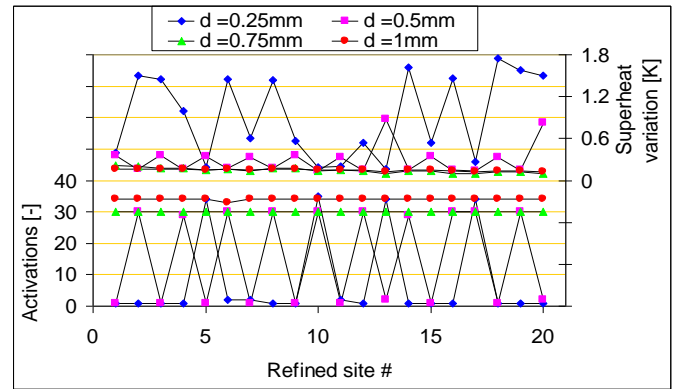
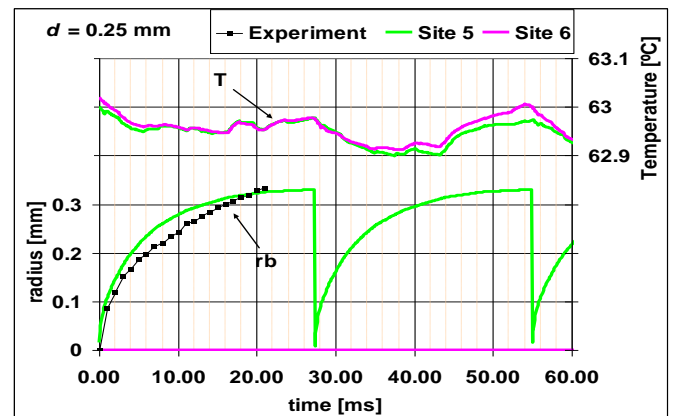**Figure 11: Activations and superheat variation for refined sites**

Figure 12: Radii and temperature histories for adjacent sites (*d* = 0.25mm)
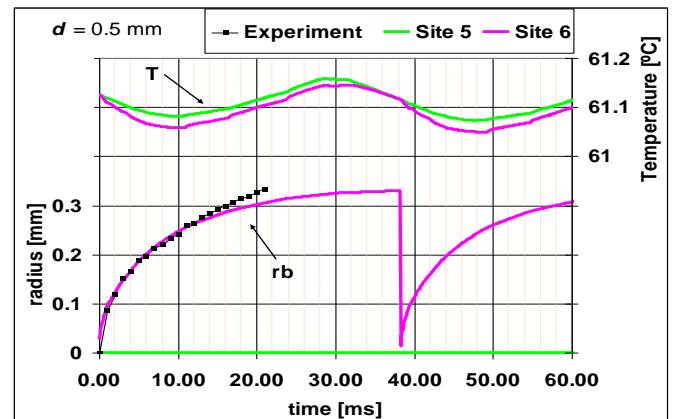
Figure 13: Radii and temperature histories for adjacent sites (*d* = 0.5mm)
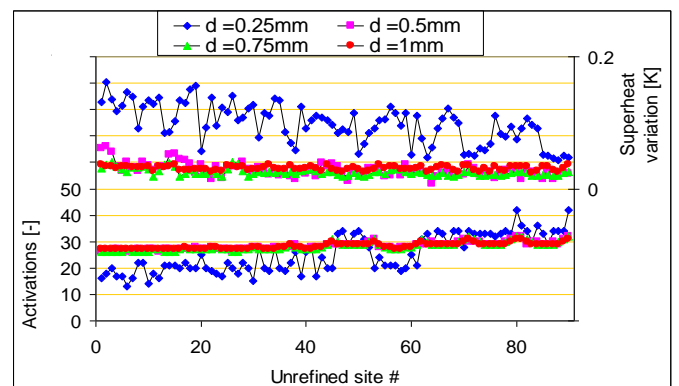
Figure 14: Activations and superheat variation for unrefined sites

analysed in order to define a new test section that will be fabricated and tested at Edinburgh University. Further experiments on this test section will provide information to improve the physical model, mostly regarding the interactions between sites on the fluid side (horizontal, declining and vertical coalescence).

SYMBOLS

d	spacing between cavities [m]
f	dimensionless factor
HTC	heat transfer coefficient [W m^{-2} K^{-1}]
p	pressure [Pa]
Δp	pressure difference [Pa]
q''	heat flux [W m^{-2}]
r	radius [m]
R	refined site
T	temperature [ºC]
ΔT	superheat [ºC]
t	time [s]
U	unrefined site
w_{xy}	cell width [m]
x, y	coordinates [m]

Greek symbols

σ	surface tension [N/m]
φ	apparent contact angle [deg]
τ_g	growth time [s]

Subscripts

0	initial condition
act	activation
b	bubble
bd	bubble departure
c	contact
C	coalescence
cav	cavity
CL	contact-line
D	dome
enh	enhanced
i, j	generic site
in	initial
loc	local
m	mesh
max	maximum
ML	micro-layer
NC	natural convection
NS	nucleation site
SEN	sensor
sat	saturation
$theor$	theoretical
w	wall

REFERENCES

1. V.K. Dhir, Mechanistic prediction of nucleate boiling heat transfer - Achievable or a hopeless task?, *Journal of Heat Transfer*, Vol. 128, pp. 1-12, 2006.

2. P. Stephan and J. Hammer, A new model for nucleate boiling heat transfer, *Journal of Heat and Mass transfer*, Vol. 30/2, pp. 119-125, 1994

3. P. Stephan and T. Fuchs, Local heat flow and temperature fluctuations in wall and fluid in nucleate boiling systems, *ECI International Conference on Boiling Heat Transfer, Spoleto*, 2006.

4. K.O. Pasamehmetoglu, and R.A. Nelson, Cavity-to-cavity interaction in nucleate boiling: effect of heat conduction within the heater, *AIChE Symposium Series (27th National Heat Transfer Conference, Minneapolis)*, Vol. 87, pp. 342-351, 1991.

5. I. Golobič, E. Pavlovič, J. von Hardenberg, M. Berry, R.A. Nelson, D.B.R. Kenning and L.A. Smith, Comparison of a mechanistic model for nucleate boiling with experimental spatio-temporal data, *Chemical Engineering Research and Design*, Vol. 82, pp. 435-444, 2004.

6. A. Sanna, C. Hutter, H.Lin, K. Sefiane, A.J. Walton, E. Pavlovič, I. Golobič, R.A. Nelson, T.G. Karayiannis and D.B.R. Kenning, Simulation and experimental investigation of pool boiling on a silicon wafer with artificial nucleation sites, *5th Eurotherm Conference on Thermal Science, Eindhoven*, 2008.

7. A. Sanna, T.G. Karayiannis, D.B.R. Kenning, C. Hutter, K. Sefiane, A.J. Walton, I. Golobič, E. Pavlovič, and R.A. Nelson, Steps towards the development of an experimentally verified simulation of pool nucleate boiling on a silicon wafer with artificial sites, *Applied Thermal Engineering*, Vol. 29, pp. 1327-1337, 2009.

8. I. Golobič, J. Petkovsek, M. Baselj, A. Papez, D.B.R. Kenning, Experimental determination of transient wall temperature distributions close to growing vapor bubbles, *Journal of Heat and Mass Transfer*, Vol. 45, pp. 857-866, 2009.

9. I. Golobič, J. Petkovsek and D.B.R. Kenning, Bubble growth and horizontal coalescence in saturated pool boiling on a thin foil, investigated by high-speed IR thermography, *Journal of Heat and Mass Transfer* (submitted), 2007.

10. J.L. Parker and M.S. El-Genk, Enhanced saturation and subcooled boiling of FC-72 dielectric liquid, *International Journal of Heat and Mass Transfer*, Vol. 48 pp. 3736-3752, 2005.

11. C. Hutter, D.B.R. Kenning, K. Sefiane, T.G. Karayiannis, H. Lin, G. Cummins and A.J. Walton, Experimental pool boiling investigations of FC-72 on Silicon with artificial cavities and integrated temperature micro-sensors, *Experimental Thermal and Fluid Science (submitted)*, 2008.

12. L. Zhang and M. Shoji, Nucleation site interaction in pool boiling on the artificial surface, *International Journal of Heat and Mass Transfer*, Vol. 46, pp. 513-522, 2003.

13. C. Hutter, A. Sanna, K. Sefiane, D.B.R. Kenning, T.G. Karayiannis, R.A. Nelson, H. Lin, G. Cummins and A.J. Walton, Experimental pool boiling investigations of vertical coalescence for FC-72 on silicon from an isolated artificial cavity, *ExHFT-07 conference, Krakow*, 2009.

14. D.B.R. Kenning, I. Golobič, H. Xing, M. Baselj, Lojk and J. von Hardenberg, Mechanistic models for pool nucleate boiling heat transfer: input and validation, *Journal of Heat and Mass Transfer*, Vol. 42, pp. 511-527, 2006.